THE ASTROPHYSICAL JOURNAL, 566:365–372, 2002 February 10

INFLUENCE OF ROTATION ON PULSAR RADIATION CHARACTERISTICS

PEYMAN AHMADI AND R. T. GANGADHARA
Indian Institute of Astrophysics, Koramangala, II Block, Bangalore 560034, India; ganga@iiap.ernet.in
Received 2001 May 29; accepted 2001 October 15

ABSTRACT

We present a relativistic model for pulsar radio emission by including the effect of rotation on coherent curvature radiation by bunches. We find that rotation broadens the width of the leading component compared to the width of the trailing component. We estimate the component widths in the average pulse profiles of about 24 pulsars and find that 19 of them have a broader leading component. We explain this difference in component widths by using the nested cone emission geometry. We estimate the effect of pulsar spin on the Stokes parameters and find that the inclination between the rotation and magnetic axes can introduce an asymmetry in the circular polarization of the conal components. We analyze the single-pulse polarization data of PSR B0329+54 at 606 MHz and find that in its conal components, one sign of circular polarization dominates in the leading component, while the other sign dominates in the trailing component. Our simulation shows that changing the sign of the impact parameter changes the sign of the circular polarization as well as the swing of the polarization angle.

Subject headings: pulsars: general — radiation mechanisms: nonthermal — radio continuum: general — stars: neutron

1. INTRODUCTION

Although a lot of effort has been devoted to understanding the pulsar radiation mechanism, it seems we still do not have a unified model for the emission mechanism and the beam structure. Three major models have been proposed for explaining the coherent radio emission from pulsars: emission by bunches (e.g., Komesaroff 1970; Sturrock 1971; Tademaru 1971; Ruderman & Sutherland 1975; Buschauer & Benford 1976, 1980; Michel 1978), relativistic plasma emission (e.g., Melrose & Gedalin 1999; Asseo & Riazuelo 2000), and maser mechanisms (e.g., Yihan et al. 1994; Malov & Chugunov 1995). Most of them make use of a secondary pair plasma and place the origin of the pulsar radiation at the inner region of the magnetosphere. However, polarization observations (e.g., Clark & Smith 1969; Blaskiewicz, Cordes, & Wasserman 1991) tend to favor curvature radiation as the emission mechanism. However, the coherent curvature emission by bunches has been criticized (e.g., Melrose 1981) for its failure to explain the creation and stability of bunches.

The rotation vector model by Radhakrishnan & Cooke (1969) has been used to interpret the average polarization-angle swing; it assumes a strong dipole magnetic field and a collimated relativistic flow of plasma. The emitted radiation is then significantly polarized along or orthogonal to the curvature of the magnetic field.

Manchester, Taylor, & Huguenin (1975) and Stinebring et al. (1984a, 1984b) have discussed polarization characteristics of single pulses and have found them to be highly polarized, with linear polarization generally dominating over circular polarization. They noted that the circular polarization sign reversal appears to occur close to the center of the subpulse. This signature is not frequency dependent, contrary to the predictions of propagation or plasma emission processes (Gangadhara, Lesch, & Krishan 1999; Gangadhara & Krishan 1993, 1995). Rankin (1983a) has studied Stokes parameters for a sample of pulsars and has shown that the circular polarization patterns are not symmetric, especially for core-dominant pulsars. Furthermore, Radhakrishnan & Rankin (1990), in their phenomenological study of the polarization properties of pulsars, clarified two extreme types of circular polarization signatures in the average profiles: (1) an antisymmetric type wherein the circular polarization changes sign in midpulse, and (2) a symmetric type wherein it is predominantly of one sign. They found a strong correlation between the position-angle swing and the change in circular polarization sign.

Rankin (1983b) suggested that core and conal emissions have different emission mechanisms, with circular polarization being a property of core emission only. Lyne & Manchester (1988) suggested that a gradual change in emission characteristics from the core region to the outer edge of the emission beam can accommodate observations better than two distinct emission processes. Han et al. (1998) have studied the circular polarization in pulsar integrated profiles and have found that the circular polarization is stronger in the central or "core" regions of the pulses, but it is not confined only to this region, as Rankin (1983a) claimed.

Although the theoretical understanding of the polarization properties of pulsar radiation is a fascinating subject, the complexity of the details has prevented a major breakthrough so far. It seems impossible to accommodate all the diverse properties of the polarization within a single radiation mechanism. Gil & Snakowski (1990) have attempted to examine the polarization properties of curvature radiation without taking into account the role of rotation. Gangadhara (1996) has estimated the energy of particles moving along rotating magnetic fields, but has not estimated the polarization of the emitted radiation. Blaskiewicz et al. (1991) have developed a model by taking into account the effect of rotation on the particle motion. They assumed a constant emission height and estimated the effect of rotation only on the position-angle swing.

In this paper, we further develop the mechanism of curvature emission by including rotation and coherency effects and estimating the polarization parameters of the emitted radiation. In this treatment, we relax the assumption of a fixed emission height made by Blaskiewicz et al. (1991). We show instead that the major observed features of the circular polarization can be explained by considering the emis-

sion from an extended region. In § 2 we introduce the equation of motion for individual particles and derive an expression for the radiation electric field. In § 3 we estimate the Stokes parameters for a coherent radiation electric field from bunches of plasma particles by assuming that the bunches are in an instantaneous circular motion along the rotating magnetic field. In § 4 we give the observational evidence in favor of predictions of our model.

2. COHERENT RADIATION FROM PLASMA

Curvature radiation from high-energy plasma particles in a strong curved magnetic field is often postulated to be the mechanism for producing radiation in the pulsar magnetosphere. The equation for particle dynamics is given by

$$\frac{d\boldsymbol{p}}{dt} = q\left(\boldsymbol{E}_i + \frac{\boldsymbol{v}}{c} \times \boldsymbol{B}\right), \tag{1}$$

where $\boldsymbol{E}_i$ is the electric field induced by the rotating magnetic field $\boldsymbol{B}$ in the pulsar magnetosphere. The symbols q, $\boldsymbol{v}$, $\boldsymbol{p}$, and c stand for particle charge, velocity, and momentum and the speed of light, respectively. Goldreich & Julian (1969) have proposed that a beam of electrons (or ions) is accelerated at the polar cap by this electric field. Sturrock (1971) suggested that this accelerated particle beam emits gamma rays by curvature radiation. These high-energy photons interact with the magnetic field and generate electron-positron pairs. The pairs thus created are most likely to be in higher Landau levels and therefore lose the perpendicular component of their momentum through synchrotron radiation. Synchrotron photons with energies above 1 MeV can further decay into electron-positron pairs in the pulsar magnetic fields.

The coherent curvature radiation from these secondary plasma particles flowing along the curved magnetic field lines is one of the important mechanisms proposed for explaining the very high brightness temperature (10^{25}–10^{30} K) from pulsars (Pacini & Rees 1970; Sturrock 1971). If $\boldsymbol{J}$ is the current density due to the flow of such a plasma, then the Fourier components of the coherent radiation electric field are given by (Jackson 1962)

$$\boldsymbol{E}(\omega) = -i\,\frac{\omega e^{i\omega R/c}}{\sqrt{2\pi}Rc^2}\int_{-\infty}^{+\infty} dt \int \hat{\boldsymbol{n}} \times (\hat{\boldsymbol{n}} \times \boldsymbol{J}) e^{i\omega(t - \hat{\boldsymbol{n}}\cdot\boldsymbol{r}/c)}\, d^3\boldsymbol{r}\,, \tag{2}$$

where R is the distance between the observer and the emission point and $\hat{\boldsymbol{n}}$ is the unit vector representing the line of sight.

Consider a stationary Cartesian coordinate system (x, y, z) as shown in Figure 1, centered on the neutron star where the z-axis is aligned with the rotation axis $\hat{\boldsymbol{\Omega}}$. Assume that $\hat{\boldsymbol{n}}$, the magnetic axis $\hat{\boldsymbol{m}}$, and $\hat{\boldsymbol{\Omega}}$ lie in the x-z plane at time $t = 0$. Consider a plasma column with an elliptical cross section flowing along the rotating magnetic field lines. Let s_0 be the length of the plasma column and ξ_0 and η_0 be the major

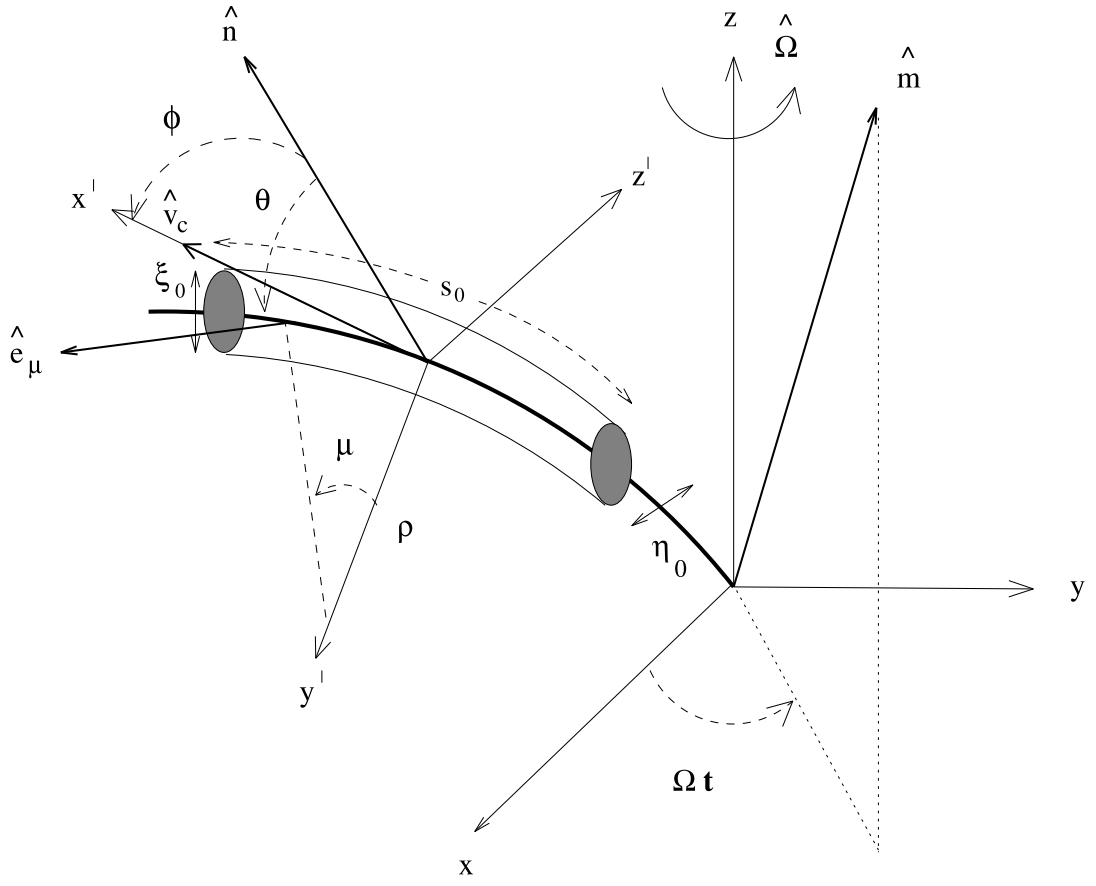

FIG. 1.—Emission region geometry. The lab frame (x, y, z) is centered on the neutron star and (x', y', z') is the comoving reference frame. The column of plasma with length s_0 and elliptical cross section with major axis ξ_0 and minor axis η_0 contains N_0 bunches of coherently radiating particles. The labels $\hat{\boldsymbol{n}}$ and $\hat{\boldsymbol{m}}$ show the line-of-sight and magnetic-dipole unit vectors, respectively.

and minor axes of its elliptical cross section, respectively. Let ζ be the angle between $\hat{\boldsymbol{\Omega}}$ and $\hat{\boldsymbol{n}}$, and let ζ_c be the angle between $\hat{\boldsymbol{\Omega}}$ and the center of momentum (CM) velocity of the plasma particles $\hat{\boldsymbol{v}}_c$. The observer receives radiation when the angle between $\hat{\boldsymbol{n}}$ and $\hat{\boldsymbol{v}}_c$ is $\leq 1/\gamma$, where γ is the Lorentz factor of the plasma bunch. The phase Ωt represents the instantaneous position of the magnetic axis $\hat{\boldsymbol{m}}$. The instantaneous plane of the CM orbit of a bunch is assumed to be an arc of a circle that makes an angle θ with the line of sight $\hat{\boldsymbol{n}}$.

In the comoving frame (x', y', z'), plasma waves (ω'_p, k'_p) are excited in the plasma column by plasma instabilities, such as the oscillating two-stream instability (Ruderman & Sutherland 1975). Since plasma waves are longitudinal, they are capable of creating density fluctuations, which can behave like particle bunches. Let ρ be the instantaneous radius of curvature of the trajectory of particles in the CM plane, μ be the angle along the arc of the trajectory measured with respect to the y'-axis that is used in the volume integration appearing in equation (2), and $\hat{\boldsymbol{e}}_\mu$ be the unit vector tangent to the trajectory. In the comoving frame, the current density and the charge density are given by

$$\boldsymbol{J}' = \hat{\boldsymbol{x}}' J'_0 \sin(k'_p x' - \omega'_p t'), \quad \sigma' = \sigma'_p \sin(k'_p x' - \omega'_p t') . \tag{3}$$

Using a Lorentz transformation, we transform the current density and charge density into the rest frame and substitute $\boldsymbol{J}$ into equation (2). Next, by integrating it we obtain

$$\boldsymbol{E}(\omega) = -i \frac{\omega e^{i\omega R/c}}{\sqrt{2\pi} R c^2} \boldsymbol{A} \tag{4}$$

and

$$\boldsymbol{A} = \frac{J_0 N s_0 \xi_0 \eta_0}{2i} \frac{\sin[(k - k_p)s_0/2]}{(k - k_p)s_0/2} \frac{\sin(k\eta_0\theta/2)}{k\eta_0\theta/2} \times \left[\hat{\epsilon}\theta\left(\frac{6\rho^2}{\omega c^2}\right)^{1/3} L_1(z) - \hat{\boldsymbol{y}}\left(\frac{36\rho}{\omega^2 c}\right)^{1/3} L_2(z)\right], \tag{5}$$

where $\hat{\epsilon} = \hat{\boldsymbol{n}} \times \hat{\boldsymbol{y}}'$, (ω, k) are the radiation frequency and wavenumber,

$$\frac{\omega'_p}{\omega_L} = \frac{\kappa\gamma}{6} + \frac{1}{2\gamma} , \tag{6}$$

and the constant κ is of the order of 10^{-3} (Buschauer & Benford 1976). The parameter

$$z = \left(\frac{6\omega^2\rho^2}{c^2}\right)^{1/3}\left(\frac{1}{2\gamma^2} + \frac{\theta^2}{2} - \frac{\omega'_p}{\gamma\omega} - \frac{\xi_0}{\rho}\right), \tag{7}$$

and for positive z, we have

$$L_1(z) = \frac{2}{3} z^{1/2} K_{1/3}[2(z/3)^{3/2}] , \tag{8}$$

$$L_2(z) = i \frac{2}{3^{3/2}} z K_{2/3}[2(z/3)^{3/2}] . \tag{9}$$

The functions $K_{1/3}$ and $K_{2/3}$ are the modified Bessel functions.

2.1. *Calculation of ρ and θ*

In the previous section we derived an expression for the Fourier components of the radiation electric field $\boldsymbol{E}(\omega)$ as a function of the radius of curvature ρ and the angle θ. Now we introduce a method for estimating these quantities in the (x, y, z) frame as functions of observable quantities such as ζ, Ωt, and the magnetic axis inclination angle α. The angular width of the open field line region above the polar cap varies as $w = (r\Omega/c)^{1/2} = (r/R_{\rm lc})^{1/2}$, where $R_{\rm lc}$ and r are the light cylinder radius and emission height, respectively. These are the field lines from which the coherent radio waves are expected to be produced. Blaskiewicz et al. (1991) have shown that in the first order of calculations, the terms of the order of w^2 are negligible in the equation of motion (eq. [1]).

We relax the assumption of an emission region confined to a constant radius made by Blaskiewicz et al. (1991) and calculate the velocity and acceleration in the CM frame of particles along the portion of magnetic field lines from which the radiation is receivable. At an arbitrary time t, the magnetic axis can be represented as

$$\hat{\boldsymbol{m}} = \sin\alpha[\hat{\boldsymbol{x}}\cos(\Omega t) + \hat{\boldsymbol{y}}\sin(\Omega t)] + \hat{\boldsymbol{z}}\cos\alpha . \tag{10}$$

In a corotating magnetosphere, the guiding center velocity of the CM is

$$\boldsymbol{v}_c \cong v_\parallel \hat{\boldsymbol{b}} + \boldsymbol{\Omega} \times \boldsymbol{r} , \tag{11}$$

where $v_\parallel$ is the velocity of the CM parallel to $\hat{\boldsymbol{b}}$, the unit vector tangent to the dipolar magnetic field lines (Hibschman & Arons 2001).

The condition for receiving the radiation is that the line of sight should lie inside the particle radiation beam with angular width $2/\gamma$, which is met when $\zeta_c \simeq \zeta$. This helps us to write $\hat{\boldsymbol{v}}_c$ as

$$\hat{\boldsymbol{v}}_c = \sin\zeta\cos\phi\hat{\boldsymbol{x}} + \sin\zeta\sin\phi\hat{\boldsymbol{y}} + \cos\zeta\hat{\boldsymbol{z}} , \tag{12}$$

since $|\hat{\boldsymbol{v}}_c - \hat{\boldsymbol{m}}|$, $|\hat{\boldsymbol{v}}_c - \hat{\boldsymbol{r}}|$, and $|\hat{\boldsymbol{m}} - \hat{\boldsymbol{r}}|$ lie inside the open field line region, and all are of the order of w. Therefore, we have

$$\hat{\boldsymbol{r}} = \frac{2}{3}\left(\hat{\boldsymbol{v}}_c - \frac{r}{c}\boldsymbol{\Omega} \times \hat{\boldsymbol{v}}_c\right)\left(1 + \frac{\epsilon^2}{18}\right) + \frac{1}{3}\left(1 + \frac{2\epsilon^2}{9}\right)\hat{\boldsymbol{m}} + O(w^3) , \tag{13}$$

where

$$\epsilon = \{\sigma^2 + 2\sin\alpha\sin\zeta[1 - \cos(\Omega t - \phi)]\}^{1/2} , \tag{14}$$

$\sigma = \zeta - \alpha$ is the impact parameter, and ϕ is the angle between $\boldsymbol{v}_c$ and $\hat{\boldsymbol{n}}$. Substituting this result for $\hat{\boldsymbol{r}}$ into equation (11) gives the CM velocity $\boldsymbol{v}_c$. Differentiating $\boldsymbol{v}_c$ with respect to time gives the acceleration

$$\boldsymbol{a} = -\frac{1}{2r}[\hat{\boldsymbol{m}}c^2 - \hat{\boldsymbol{v}}_c(\hat{\boldsymbol{v}}_c \cdot \hat{\boldsymbol{m}})c^2 - 3cr\Omega(\hat{\boldsymbol{z}} \times \hat{\boldsymbol{v}}_c)] + O(w^3) . \tag{15}$$

The instantaneous radius of curvature of a particle orbit is given by

$$\rho = \frac{v_c^2}{a} \cong \frac{2r}{[\epsilon^2 - (6r\Omega/c)\sin\alpha\sin\zeta\sin(\Omega t - \phi)]^{1/2}} . \tag{16}$$

The angle θ between the line of sight and the instantaneous plane of orbit is given by

$$\sin\theta = \hat{\boldsymbol{n}} \cdot (\hat{\boldsymbol{v}}_c \times \hat{\boldsymbol{a}}) \tag{17}$$

or

$$|\boldsymbol{a}| \sin\theta = \sin\zeta[\sin\zeta \sin\phi \cos\alpha - \cos\zeta \sin\alpha \sin(\Omega t)] + \sin\zeta \cos\zeta \times [\sin\alpha \cos\phi \sin(\Omega t) - \sin\alpha \sin\phi \cos(\Omega t)] - 3r\Omega \cos\beta \sin^2\beta[1 - \cos(\Omega t)]/c\,, \quad (18)$$

where $|\boldsymbol{a}|$ is the magnitude of acceleration. Equations (16) and (18) specify ρ and θ as functions of pulse phase. Substituting these relations into equation (2) gives $\boldsymbol{E}(\omega)$ as a function of the rotation phase. From equations (16) and (18), we infer the following:

1. If ρ_l is the curvature of particle trajectory on the leading side ($\Omega t - \phi < 0$) and ρ_t is the curvature on the trailing side ($\Omega t - \phi > 0$), then equation (16) shows that $\rho_l < \rho_t$.
2. For phases $\pm\phi$ on either side of the orbital plane, which is at $\phi = 0$, equation (18) shows that θ is asymmetric, i.e., the values of θ are not same at $\pm\phi$.

2.2. *Stokes Parameters*

Let $E_y(\omega)$ and $E_\epsilon(\omega)$ be the components of the radiation electric field $\boldsymbol{E}(\omega)$ given by equation (4). Then, the Stokes parameters can be defined as

$$I = E_y E_y^* + E_\epsilon E_\epsilon^* = W^2 D^2 S^2 \left\{ \frac{4}{27}\left(\frac{36\rho}{\omega^2 c}\right)^{2/3} z^2 K_{2/3}[2(z/3)^{3/2}]^2 + \theta^2 \left(\frac{6\rho^2}{\omega c^2}\right)^{2/3}\left(\frac{4}{9}\right) z K_{1/3}[2(z/3)^{3/2}]^2 \right\}, \quad (19)$$

$$Q = E_y E_y^* - E_\epsilon E_\epsilon^* = W^2 D^2 S^2 \left\{ \frac{4}{27}\left(\frac{36\rho}{\omega^2 c}\right)^{2/3} z^2 K_{2/3}[2(z/3)^{3/2}]^2 - \theta^2 \left(\frac{6\rho^2}{\omega c^2}\right)^{2/3}\left(\frac{4}{9}\right) z K_{1/3}[2(z/3)^{3/2}]^2 \right\}, \quad (20)$$

$$U = 2\mathrm{Re}(E_y E_\epsilon^*) = 0\,, \quad (21)$$

$$V = 2\mathrm{Im}(E_y E_\epsilon^*) = -2W^2 D^2 S^2 \left(\frac{36\rho}{\omega^2 c}\right)^{1/3}\left(\frac{6\rho^2}{\omega c^2}\right)^{1/3}\left(\frac{4}{3^{5/2}}\right) \times \theta z^{3/2} K_{2/3}[2(z/3)^{3/2}] K_{1/3}[2(z/3)^{3/2}]\,, \quad (22)$$

where

$$W = \frac{J_0 N_0 S_0 \xi_0 \eta_0}{2}\,, \quad D = \frac{\sin(k\eta_0\theta/2)}{k\eta_0\theta/2}\,, \quad S = \frac{\sin[(k - k_p)s_0/2]}{(k - k_p)s_0/2}\,, \quad (23)$$

and where N_0 is the number of radiating bunches in a column. The polarization position angle is defined as

$$\psi = \frac{1}{2}\tan^{-1}\left(\frac{U}{Q}\right). \quad (24)$$

Since U is zero, ψ can be zero or $\pi/2$. However, $\psi = \pi/2$ represents the real orientation of $\boldsymbol{E}(\omega)$ as predicted by equation (2). Note that because of the special choice of the coordinate system $(\hat{\epsilon}, \hat{\boldsymbol{y}}, \hat{\boldsymbol{n}})$ attached to the CM, ψ becomes constant for a given field line. However, when the line of sight moves from field line to field line because of rotation, the polarization position angle swings in agreement with the rotation vector model (Radhakrishnan & Cooke 1969). In the (x, y, z) coordinate system, the position angle is the angle between the radiation electric field and the projected spin axis on the plane of sky. Since the particle acceleration $\boldsymbol{a}$ is parallel to $\boldsymbol{E}$, we use $\boldsymbol{a}$ as the reference for convenience. Since $\hat{\boldsymbol{n}}$ is normal to both the plane of sky and $\hat{\boldsymbol{y}}$, the plane of sky contains the y-axis. Hence, the linear polarization angle ψ can be estimated from

$$\tan\psi = \frac{\hat{\boldsymbol{a}} \cdot \hat{\boldsymbol{y}}}{\hat{\boldsymbol{a}} \cdot (\hat{\boldsymbol{n}} \times \hat{\boldsymbol{y}})}\,. \quad (25)$$

After substituting for $\hat{\boldsymbol{a}}$, it can be simplified as

$$\psi = \tan^{-1}\left[\frac{3(r\Omega/c)\sin\zeta - \sin\alpha \sin(\Omega t)}{\sin\sigma + \sin\alpha \cos\zeta[1 - \cos(\Omega t)]}\right]. \quad (26)$$

3. NUMERICAL CALCULATION

For numerical calculations, we adopt the values of emission heights and component locations provided recently by Gangadhara & Gupta (2001) for PSR B0329+54 at 606 MHz. Even though they have proposed nine emission components, we consider only three strong components, marked as i, iii, and iv in Figure 4*a*, which have higher polarization. Out of these three, iii is a core component, and i and iv are the conal components of cone number 3 (Gangadhara & Gupta 2001). The phase locations of components i and iv are $-12.^\circ6 \pm 0.^\circ64$ and $9.^\circ5 \pm 0.^\circ64$, respectively. They assumed zero pulse phase for the core; however, the core is expected to be produced at some height above the polar cap and is most likely to be shifted from zero pulse phase to the trailing side because of aberration and retardation. In our calculation, we assume the core component is emitted at a height of $r_{\rm core} \simeq 2r_{\rm ns} \simeq 20$ km above the polar cap.

The dipole magnetic field strength of PSR B0329+54 is about $B_0 = 1.2 \times 10^{12}$ G at the surface of the neutron star. Using the characteristic curvature radiation frequency given by $\omega_c = (3/2)\gamma^3(c/\rho)$, we can estimate the particle Lorentz factor γ. For $\nu_c = \omega_c/(2\pi) = 606$ MHz and emission height $r_{\rm cone} = 600 \pm 180$ km, equation (16) gives $\rho_l \simeq 10^4 \pm 10^3$ km and $\rho_t \simeq (2 \times 10^4) \pm 10^3$ km. For these values, we find $\gamma = 300 \pm 190$ for the leading component i and 480 ± 60 for the trailing component iv. Having an estimate of the particles' Lorentz factor, we compute the Stokes parameters using equations (19)–(22).

The coherency factor S^2 (eq. [23]) becomes maximum for $k \simeq k_p$, i.e., the coherency is more effective when the radiation wavenumber is of the order of the plasma wavenumber. We use this resonant matching condition in our numerical calculation of polarization parameters. The diffraction term D^2 takes a maximum value $\simeq 1$ for the parameters used in our calculations. Furthermore, since the radius of curvature is much greater than the plasma column height ξ_0, the last term on the right hand side of equation (7) is negligible compared to the other terms.

Figure 2 shows the results of the numerical estimation of intensity I, linear polarization $L = (Q^2 + U^2)^{1/2}$, circular polarization V, and linear polarization angle ψ. To calculate the polarization of each component in this figure, we

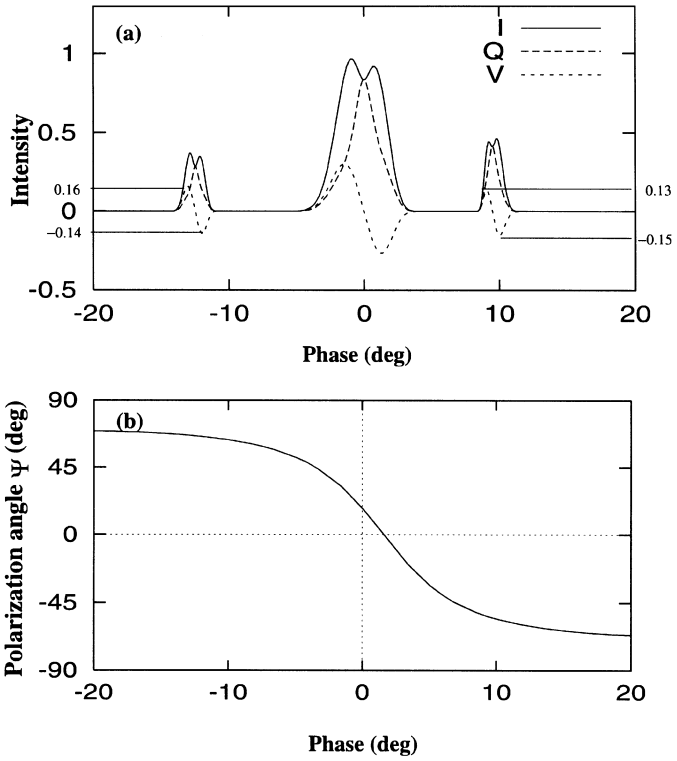

FIG. 2.—(*a*) Normalized Stokes parameters, *I*, *L*, and *V*. (*b*) Polarization angle for a single pulse, simulated using $\alpha = 30°$, $\sigma = 2.°5$, $\omega_L = \omega_r/3$, and $\omega_r = 610$ MHz.

considered a bunch of field lines with a proper rotation phase. The main features of Figure 2 are the following:

1. The asymmetry in the phase location of conal components i and iv with respect to the core iii arises because of the fact that the emission height of the conal components is higher than the core component, which is explained as an aberration and retardation effect by Gangadhara & Gupta (2001). Since Blaskiewicz et al. (1991) considered a constant emission height, they could estimate only the influence of aberration on the pulse width, but not of retardation. However, we have relaxed the assumption of constant emission height by estimating the emission over a range of height, where the conditions are conducive for coherent curvature emission. So, we are able to estimate the change in component widths due to both aberration and retardation, which is almost double the value predicted by Blaskiewicz et al. (1991).

2. Figure 2*a* shows that the phase width of component i is broader than that of component iv. This broadening is a consequence of ρ_l becoming smaller than ρ_t. We propose that this result has observational evidence. In the next section we analyze the component widths of 24 pulsars to check this prediction.

3. As we expected from our discussion on the radius of curvature, with similar particle densities on the field lines, the Stokes parameter *I* for the trailing component becomes stronger than that of the leading component, in agreement with Jackson (1962, eq. 14.93).

4. If we define the clockwise rotation of $\boldsymbol{E}(\omega)$ as negative circular polarization ($V < 0$) and counterclockwise rotation as positive circular polarization ($V > 0$), then Figure 2*a* shows that all three components (i, iii, and iv) display the well-known antisymmetric type of circular polarization. However, there is a difference in the relative magnitudes of circular polarization on either side of each component center, i.e., positive *V* dominates over negative *V* in the case of component i, while in component iv, negative *V* dominates. This happens because of the fact that due to the inclination of the plane of field lines with respect to the rotation axis, while observing, e.g., component i, we tend to receive more radiation from the leading side of the plane of any given field line (associated with that component) compared to that received from the trailing side of the same field line.

In the case of the core component, the planes of the magnetic field lines are nearly parallel to the rotation axis. Therefore, we tend to equally receive both positive and negative parts of circular polarization from either side of the field line planes. Hence, circular polarization becomes antisymmetric for the core component.

Furthermore, the circular polarization is affected by rotation in such a way that in the case of the leading component, it makes positive *V* weaker, but in the case of the trailing component, it enhances negative *V*. The simulated curve representing *V* in Figure 2*a* depicts this behavior.

5. Figure 2*b* shows the polarization-angle swing with respect to pulse phase. It shows that the centroid of the polarization-angle curve shifts toward the trailing side. This shift arises because of the rotation as proposed by Blaskiewicz et al. (1991). However, Hibschman & Arons (2001) have shown that current flow above the polar cap can shift the polarization swing in the opposite direction.

6. For the purpose of comparison, we repeated the calculation of the Stokes parameters by changing the impact parameter to $-2.°5$, and plotted them in Figure 3*b*. We notice that the change of the impact parameter σ flips the polarization-angle swing and sign of circular polarization.

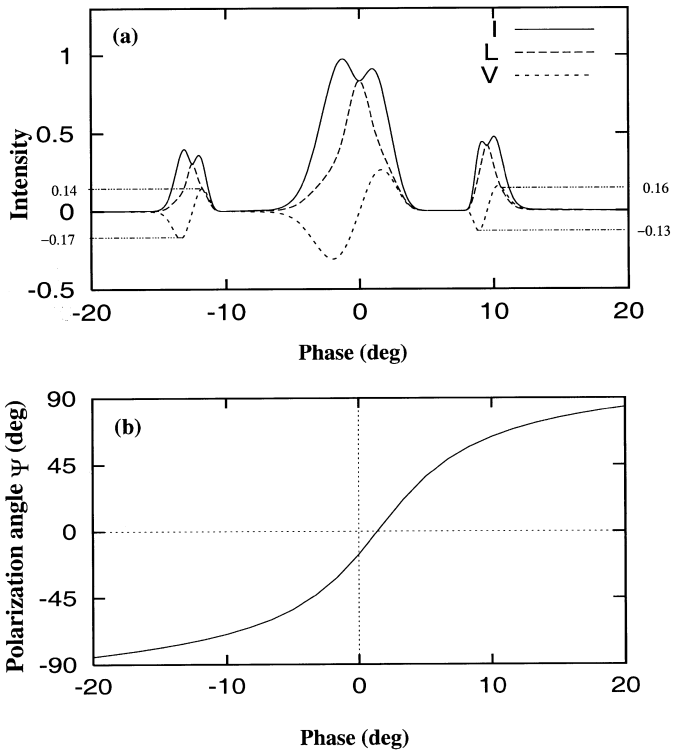

FIG. 3.—(*a*) Normalized Stokes parameters, *I*, *L*, and *V*. (*b*) Polarization angle for a single pulse, simulated using $\alpha = 30°$, $\sigma = -2.°5$, $\omega_L = \omega_r/3$, and $\omega_r = 610$ MHz.

4. OBSERVATIONAL EVIDENCES

Our model predicts that due to rotation, the width of the leading component becomes broader than the width of the trailing component. Furthermore, the circular polarization of the leading component is dominantly in one sign, while on the trailing component, the other sign dominates. To find the observational evidence in this regard, we analyzed the average profiles of about 24 pulsars and also the single-pulse polarimetric data of PSR B0329+54.

4.1. *Effect of the Rotation on Component Width*

We estimated the component widths on the trailing and leading sides of the average profiles of 24 pulsars using the data available in EPN format on the Web. We compared the full width at half-maxima for the leading component ($FWHM_l$) and the trailing component ($FWHM_t$) of each pulsar. To select our sample, we considered the following criteria: (1) The pulse profile should not change drastically over the range of 600–1000 MHz, i.e., the pulse profile should be stable throughout this range of frequencies. (2) The conal components should be prominent and not affected by the presence of the core component. (3) The leading and trailing components should be distinguishable enough that we can fit Gaussians to them without ambiguity.

According to Rankin's (1990) classification, the best candidates for our sample are conal double, triplet and multiple pulsars. We choose eight of the pulsars referred to as "double conal" in Rankin (1990) and do not consider sources such as PSR B1133+16 because they may have weaker components than the visible components in the average pulse profiles (Nowakowski 1996).We found the $FWHM_l$ and $FWHM_t$ by fitting Gaussians to the pulse components, and estimated their ratios. We did this analysis at different frequencies for each pulsar and present only the results at 610 MHz, except for a few sources for which the data was not available at this frequency. Table 1 shows the ratio of $FWHM_l$ to $FWHM_t$ for a sample of 24 pulsars. It shows that 19 out of 24 pulsars have a broader leading component than a trailing one. Of course, for sources such as PSR B0834+06, most likely a core component exists close to the trailing component, and consequently it is broader than the leading component.

We performed a Kolmogorov-Smirnov test on two data sets, comprised of the leading-side component widths for one, and the trailing-side component widths for the other. The mean component widths were 5°.83 and 5°.06 for the leading and the trailing components, respectively. The Kolmogorov-Smirnov statistic D was found to be 0°.17, and the significance level P was 0°.86. The 95% confidence interval for the actual mean widths were 3°.24 and 2°.71 for the leading and trailing components, respectively.

TABLE 1

PULSE WIDTH COMPARISON

PSR B	Frequency (MHz)	Period (s)	$FWHM_l/FWHM_t$	Reference
0052+51...	610	2.115	1.032 ± 2.20E−02	1
0059+65...	610	1.679	1.052 ± 2.22E−02	1
0148−06...	610	1.465	1.136 ± 7.49E−03	1
0226+70...	610	1.467	1.3574 ± 0.0	1
0301+19...	610	1.388	0.937 ± 0.0	1
0525+21...	610	3.746	1.056 ± 0.0	1
0559−05...	610	0.396	1.772 ± 0.0	1
0818−41...	660	0.545	1.319 ± 2.85E−02	3
0834+06...	4800	1.274	0.868 ± 2.0	4
1254−10...	610	0.617	1.106 ± 2.59E−02	1
1601−52...	138	0.658	1.178 ± 6.24	3
1648−17...	606	0.973	1.190 ± 0.0	1
1800−21...	1642	0.134	0.850 ± 3.58E−02	1
1822−09...	610	0.769	1.141 ± 0.0	1
1823−13...	1642	0.101	1.190 ± 9.98E−02	1
1839−04...	606	1.840	1.442 ± 9.10E−03	1
1914+09...	610	0.270	1.628 ± 0.0	1
1919+21...	610	1.337	1.111 ± 0.0	1
1935+25...	606	0.201	0.839 ± 0.0	1
1942−00...	646	1.046	1.354 ± 3.90	2
2020+28...	610	0.343	1.150 ± 0.0	1
2044+15...	610	1.138	1.572 ± 1.45E−02	1
2053+21...	606	0.815	0.920 ± 0.0	1
2224+65...	610	0.682	1.025 ± 8.98E−03	1

REFERENCES.—(1) Gould & Lyne 1998; (2) Kaspi et al. 1996; (3) Qiao et al. 1995; (4) Kijak et al. 1997.

4.2. *Interpretation of Circular Polarization from PSR B0329+54*

To study the nature of circular polarization from PSR B0329+54, we analyzed the single-pulse data at 606 MHz taken on 1996 August 30 from the Lovell telescope at Jodrell Bank. We considered about 2500 single pulses with a time resolution of 0.249 ms. The average polarization parameters, intensity I, linear L, and circular V polarization, are plotted as functions of pulse phase in Figure 4*a*. The solid curve indicates I, while the dashed and dotted ones represent L and V, respectively, in arbitrary units. The average polarization angle (*filled circles*) is given in Figure 4*b*.

The gray-scale maps in Figures 4*b*–4*d* show the frequency of the occurrence of polarization parameters with respect to the pulse phase in single pulses. We used the PGPLOT routines developed by Pearson (1989) for making gray-scale maps. The FORTRAN subroutine PGGRAY draws a gray-scale map of an array of the polarization parameters versus phase by determining the shade of each point from the corresponding array value. The shade is a number in the range from 0 to 1 obtained by linear interpolation between the background level (*white*) and the foreground level (*black*). The white regions in the maps have shade = 0 and the darkest regions have shade = 1. This technique has become a powerful tool in analyzing pulsar polarization properties (e.g., Stinebring et al. 1984a, 1984b). Figures 4*b*, 4*c*, and 4*d* show the polarization angle and linear and circular polarization gray-scale maps, respectively.

The darkest shades represent the most probable regions of occurrence. The gray-scale maps were made from all the phase bins in which the linear polarization L was above the 4 σ level. Here σ is the rms of L in the off-pulse region. All the phase bins in which the condition $L^2 + V^2 \leq I^2$ was not met were excluded, since they led to spurious polarization quantities.

The average circular polarization was obtained from the gray-scale map (Fig. 4*d*) and the solid curve superposed in Figure 4*d*. Note that for the sake of plotting on the selected scale, the whole curve has been amplified by a factor of 5. It shows that under the leading component i, the circular polarization is positive, and under the trailing component iv, it is negative, while it is antisymmetric under the core.

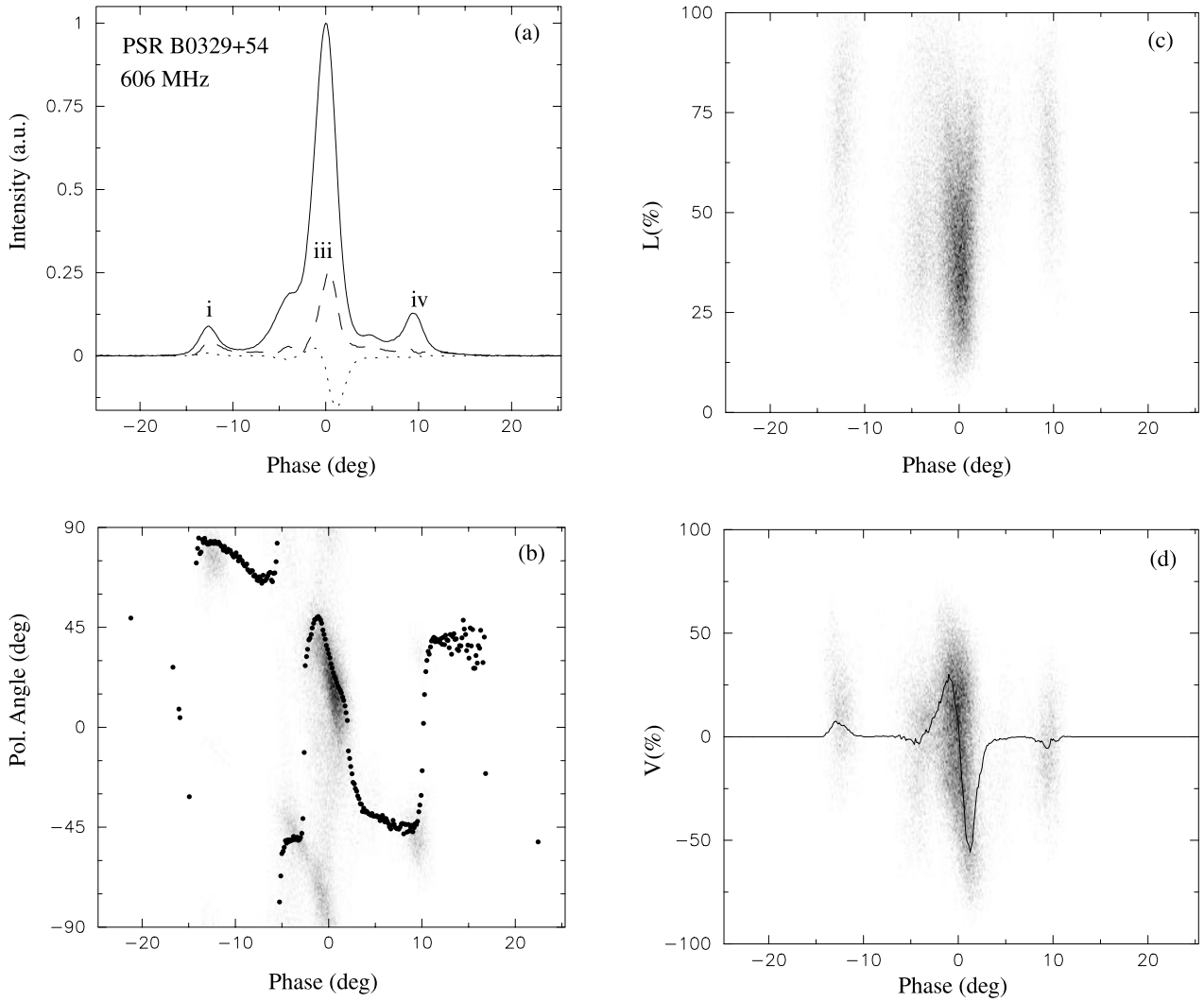

FIG. 4.—(*a*) Average pulse profile of PSR B0329+54 with arbitrary intensity units (a.u.). (*b*) Average polarization angle ψ (*filled circles*) and polarization-angle gray-scale map obtained from individual pulses. Panels (*c*) and (*d*) represent the gray-scale maps of L (%) and V (%), respectively. The shade is a number in the range 0 (*white*) to 1 (*black*), obtained by linear interpolation between the background and foreground levels. The average circular polarization curve (*solid line*) is superposed in panel (*d*).

This type of circular polarization can be explained by considering dipolar magnetic field lines with an inclined magnetic axis with respect to the rotation axis. In agreement with this observational result, our Figure 2*a* shows the dominance of positive circular polarization under the leading component and of negative under the trailing component, with antisymmetric polarization under the core.

5. CONCLUSION

We have calculated the Stokes parameters I, Q, and V for pulsar radio emission by taking into account the effect of the neutron star's spin for the first time. Figures 2*a* and 3*a* show that under the influence of rotation, the intensity I for the leading component becomes less than that of the trailing component for a similar distribution of emitting particles on different field lines.

According to the conal model (Rankin 1983a, 1983b, 1990, 1993), the emission regions on the polar cap are organized in concentric hollow cones. Our simulation shows that the leading component becomes broader than its trailing counterpart. This broadening is induced by rotation through a change in the curvature of particle trajectories, as discussed in § 3. By analyzing 24 pulsar pulse profiles, we find that 19 of them have leading components broader than trailing ones, and thereby confirm the possibility of detecting such an effect through observations. We note that such a broadening becomes observable only when the emission components are organized in the form of nested cones.

We have found that due to the inclination of the magnetic axis with respect to the rotation axis and the alteration of particle trajectories by rotation, one sign of circular polarization becomes stronger in the conal components of single pulses. Because of this enhancement of one sign of circular polarization in single pulses, one sign of circular polarization survives in the conal components of an average pulse profile. It is worth mentioning that the inclination of magnetic field planes with respect to the line of sight is mainly responsible for the enhancement of one sign of circular polarization in the conal component. However, in the case

of the core component, this effect vanishes, and consequently leads to circular polarization with an antisymmetric profile.

Radhakrishnan & Rankin (1990) found a strong correlation between the direction of polarization-angle swing and the change in sign of circular polarization. Our simulation shows that changing the sign of the impact parameter flips the sign of the circular polarization and polarization-angle swing. Therefore, the above correlation is caused by a change in the sign of the impact parameter. The centroid of the polarization-angle curve does not coincide with the pulse center as a consequence of rotation.

We thank Y. Gupta and V. Krishan for carefully reading the manuscript and making comments. Also, we are grateful to A. G. Lyne for providing the Jodrell Bank data of PSR B0329+54. Part of this research has made use of the EPN database maintained by the Max Planck Institut für Radio Astronomie on the Web.

REFERENCES

Asseo, E., & Riazuelo, A. 2000, MNRAS, 318, 983
Blaskiewicz, M., Cordes, J. M., & Wasserman, I. 1991, ApJ, 370, 643
Buschauer, R., & Benford, G. 1976, MNRAS, 177, 109
———. 1980, MNRAS, 190, 945
Clark, R. R., & Smith, F. G. 1969, Nature, 221, 724
Gangadhara, R. T. 1996, A&A, 314, 853
Gangadhara, R. T., & Gupta, Y. 2001, ApJ, 555, 31
Gangadhara, R. T., & Krishan, V. 1993, ApJ, 415, 505
———. 1995, ApJ, 440, 116
Gangadhara, R. T., Lesch, H., & Krishan, V. 1999, MNRAS, 307, 830
Gil, J. A., & Snakowski, J. K. 1990, A&A, 234, 237
Goldreich, P., & Julian, W. H. 1969, ApJ, 157, 869
Gould, D. M., & Lyne, A. G. 1998, MNRAS, 301, 235
Han, J. L., Manchester, R. N., Xu, X. A., & Qiao, J. G. 1998, MNRAS, 300, 373
Hibschman, J. A., & Arons, J. 2001, ApJ, 546, 382
Jackson, J. D. 1962, Classical Electrodynamics (New York: Wiley)
Kaspi, V. M., Johnston, S., Manchester, R. N., Stairs, I., Crawford, F., Lyne, A. G., & D'Amico, N. 1996, AJ, 111, 2028
Kijak, J., Kramer, M., Wielebinski, R., & Jessner, A. 1997, A&A, 318, L63
Komesaroff, M. M. 1970, Nature, 225, 612
Lyne, A. G., & Manchester, R. N. 1988, MNRAS, 234, 477
Malov, D. E., & Chugunov, Yu. V. 1995, Astron. Rep., 39, 625
Manchester, R. N., Taylor, J. H., & Huguenin, G. R. 1975, ApJ, 196, 83
Melrose, D. B. 1981, in IAU Symp. 95, Pulsars, ed. W. Sieber & R. Wielebinski (London: Reidel), 133
Melrose, D. B., & Gedalin, M. E. 1999, ApJ, 521, 351
Michel, F. C. 1978, ApJ, 220, 1101
Nowakowski, A. L. 1996, ApJ, 457, 868
Pacini, F., & Rees, M. J. 1970, Nature, 226, 622
Pearson, T. J. 1989, PGPLOT Graphics Subroutine Library (version 4.9; Pasadena: Caltech)
Qiao, G., Manchester, R. N., Lyne, A. G., & Gould, D. M. 1995, MNRAS, 274, 572
Radhakrishnan, V., & Cooke, D. J. 1969, ApJ, 3, L225
Radhakrishnan, V., & Rankin, J. M. 1990, ApJ, 352, 258
Rankin, J. M. 1983a, ApJ, 274, 333
———. 1983b, ApJ, 274, 359
———. 1990, ApJ, 352, 247
———. 1993, ApJS, 85, 145
Ruderman, M. A., & Sutherland, P. G. 1975, ApJ, 196, 51
Stinebring, D. R., et al. 1984a, ApJS, 55, 247
———. 1984b, ApJS, 55, 279
Sturrock, P. A. 1971, ApJ, 164, 529
Tademaru, E. 1971, Ap&SS, 12, 193
Yihan, Z., Dingyi, M., Deyu, W., & Xinji, W. 1994, A&A, 282, 467